HHS Public Access

Author manuscript

ACS Catal. Author manuscript; available in PMC 2024 August 26.

Published in final edited form as:

ACS Catal. 2023 November 03; 13(21): 14368–14376. doi:10.1021/acscatal.3c03538.

Elucidation of the α-Ketoamide Inhibition Mechanism: Revealing the Critical Role of the Electrostatic Reorganization Effect of Asp17 in the Active Site of the 20S Proteasome

Jiao Zhou,
Ciechanover Institute of Precision and Regenerative Medicine, School of Medicine, Chinese University of Hong Kong, Shenzhen 518172, China;

Xiaohong Sang,
Ciechanover Institute of Precision and Regenerative Medicine, School of Medicine, Chinese University of Hong Kong, Shenzhen 518172, China;

Juan Wang,
School of Life Sciences, Tsinghua University, Beijing 100084, China

Yan Xu,
Ciechanover Institute of Precision and Regenerative Medicine, School of Medicine, Chinese University of Hong Kong, Shenzhen 518172, China;

Department of Medicine, Division of Infectious Diseases and Global Public Health, School of Medicine, University of California at San Diego, La Jolla, California 92037, United States

Jing An,
Department of Medicine, Division of Infectious Diseases and Global Public Health, School of Medicine, University of California at San Diego, La Jolla, California 92037, United States

Zhen Tao Chu,
Department of Chemistry, University of Southern California, Los Angeles, California 90089, United States

Arjun Saha,

Corresponding Authors: Arjun Saha – Department of Chemistry & Biochemistry, University of Wisconsin-Milwaukee, Milwaukee, Wisconsin 53213, United States; saha6@uwm.edu, **Arieh Warshel** – Department of Chemistry, University of Southern California, Los Angeles, California 90089, United States; warshel@usc.edu, **Ziwei Huang** – Ciechanover Institute of Precision and Regenerative Medicine, School of Medicine, Chinese University of Hong Kong, Shenzhen 518172, China; School of Life Sciences, Tsinghua University, Beijing 100084, China; Department of Medicine, Division of Infectious Diseases and Global Public Health, School of Medicine, University of California at San Diego, La Jolla, California 92037, United States; zhuang@health.ucsd.edu.

Supporting Information

The Supporting Information is available free of charge at https://pubs.acs.org/doi/10.1021/acscatal.3c03538.

The energy contributions of each residue for the Bsc2189-proteasome noncovalent complex; structure of end frames for each step along the PnoncovNP reaction pathway; the relaxed structures before the PT2 step and NA2; the possibility of a concerted mechanism; the predicted pK_a values; calculated and experimental binding free energies of the covalent proteasome–Bsc2189 complexes; scheme for PT1 showing EVB atom numbers; the partial charges of region I atoms used for the PT1; scheme for NA2 showing EVB atom numbers; the partial charges of region I atoms used for the NA2 step; scheme for PT2 showing EVB atom numbers; the partial charges of region I atoms used for the PT2 step; scheme for PT3 showing EVB atom numbers; the partial charges of region I atoms used for the PT3 step; scheme for NA3 showing EVB atom numbers; the partial charges of region I atoms used for the NA3 step; and EVB calibration parameters (PDF)

Complete contact information is available at: https://pubs.acs.org/10.1021/acscatal.3c03538

The authors declare no competing financial interest.

Department of Chemistry & Biochemistry, University of Wisconsin-Milwaukee, Milwaukee, Wisconsin 53213, United States;

Arieh Warshel,
Department of Chemistry, University of Southern California, Los Angeles, California 90089, United States;

Ziwei Huang
Ciechanover Institute of Precision and Regenerative Medicine, School of Medicine, Chinese University of Hong Kong Shenzhen 518172, China;

School of Life Sciences, Tsinghua University, Beijing 100084, China;

Department of Medicine, Division of Infectious Diseases and Global Public Health, School of Medicine, University of California at San Diego, La Jolla, California 92037, United States;

Abstract

The 20S proteasome is an attractive drug target for the development of anticancer agents because it plays an important role in cellular protein degradation. It has a threonine residue that can act as a nucleophile to attack inhibitors with an electrophilic warhead, forming a covalent adduct. Fundamental understanding of the reaction mechanism between covalent inhibitors and the proteasome may assist the design and refinement of compounds with the desired activity. In this study, we investigated the covalent inhibition mechanism of an α-keto phenylamide inhibitor of the proteasome. We calculated the noncovalent binding free energy using the PDLD/S-LRA/β method and the reaction free energy through the empirical valence bond method (EVB). Several possible reaction pathways were explored. Subsequently, we validated the calculated activation and reaction free energies of the most plausible pathways by performing kinetic experiments. Furthermore, the effects of different ionization states of Asp17 on the activation energy at each step were also discussed. The results revealed that the ionization states of Asp17 remarkably affect the activation energies and there is an electrostatic reorganization of Asp17 during the course of the reaction. Our results demonstrate the critical electrostatic effect of Asp17 in the active site of the 20S proteasome.

Graphical Abstract

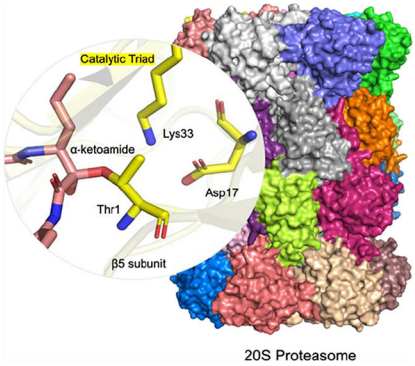

Keywords

20S proteasome; α-ketoamide; inhibition mechanism; electrostatic reorganization; catalytic triad; EVB

INTRODUCTION

The ubiquitin-proteasome system (UPS) is an intricate molecular machine of protein homeostasis in cells.[1,2] Proteasome is the core catalytic particle of the UPS taking charge of protein degradation.[3] The proteasome is widely expressed in the cytosol and nucleus and has a myriad of functions in cells, including degradation of misfolded proteins, regulation of the cell cycle, cancer progression, and inflammatory and immune responses. The proteasome has been shown to be a valuable drug target for treating multiple myeloma (MM), a hematological malignancy.[4,5] To date, three proteasome inhibitors have been approved for clinical use in patients with MM.[6] Bortezomib is the first-generation proteasome inhibitor approved in 2003 that paved the way for the investigation of the druggable proteasome.

α-Ketoamide is a novel kind of reversible covalent proteasome inhibitor with several advantages.[7] The crystal structures show that its phenylamide moiety projects into the primed site (S1′) that was rarely investigated in past drug development efforts (Figure 1).[8] Previous studies imply that optimization of the α-keto phenylamide with different substitutions at its phenyl group increases the β5 binding potency and reduces the adverse events, such as peripheral neuropathy.[9,10] Exploiting the primed site has been shown as an effective strategy for improving the specificity and potency of protease inhibitors.[11–13] Furthermore, α-ketoamide's electrophile shows a reversible inhibition against the enzyme with the potential for the treatment of solid tumors.[14] The reversible inhibition may make it a safer option compared to irreversible covalent inhibitors.[15] Thus, it is worth optimizing further α-ketoamides to develop efficient proteasome inhibitors with better pharmacological properties.

The mechanism of α-ketoamide forming a covalent adduct with the 20S proteasome is not yet delineated. Detailed understanding of the reaction mechanism of such covalent inhibitors would be helpful in designing agents with high potency. To date, the opinions about the catalytic center of the 20S proteasome are controversial for computational scientists. Initially, Wei et al. investigated the proteolysis mechanism of the substrate (e.g., Suc-LLVY-AMC) as well as the mechanism of covalent inhibition for different inhibitors (e.g., epoxomicin and syringgolin A) and suggested Thr1 as the catalytic residue.[16–18] As demonstrated in their studies, the termini amino group of Thr1 acts as the general base for Thr1O$^{\gamma}$ activation. Later, Huber et al. combined mutagenesis and X-ray crystallographic studies to put forward a catalytic triad for the catalysis consisting of Thr1, Lys33, and Asp17 residues.[19] In their study, a significantly reduced substrate and inhibitor activity for the β5-Lys33Ala variant confirmed that Lys33 initiates the reaction by deprotonating the Thr1 hydroxyl group. Moreover, there is a water molecule occupying the position normally taken by Lys33-NH_2, which forms hydrogen bonds with the side chains of Thr1O$^{\gamma}$ and Asp170$^{\delta}$ in the crystal structure of the β5-K33A mutant. This well-defined solvent

molecule implied the general base function of Lys33. Although the β5-D17N mutant also provokes a severe defect in the enzyme activity, the role of Asp17 has not received its due importance.[20–23] Since then, most researchers recognized the importance of Lys33 and provided a unified view of the Thr1-Lys33 catalytic dyad for enzyme activity. Very recently, Serrano-Aparicio et al. clarified the critical role of the Asp17-Lys33 dyad through the analysis of the electrostatic features of the active site of the 20S proteasome[24]

EXPERIMENTAL METHODS

Preparation of the Modeling System.

The catalytically active center of the 20S proteasome β5 subunit is only related to the β5 and β6 subunits, and the other subunits have little effect on the chymotrypsin-like activity.[23] The K (β5) and L (β6) chains in PDB entry 4NO8 were retained as the main simulation system. The structure used (PDB 4NO8) is the only reported complex structure, including the α-ketoamide inhibitor we investigated. The inhibitor in the PDB named Bsc2189 was used as the a-keto phenylamide inhibitor in this study. The covalent bond between the inhibitor and residue Thr1 was removed. The inhibitor was then added hydrogens and was energy minimized using SYBYL-X. The partial charges of the inhibitor were evaluated at the B3LYP/6–311d(d,p) level using Gaussian 09.[28] The calculated charges were then fitted to obtain the restrained electrostatic potential (RESP) charges using Antechamber.[29] The amino group of the side chain of Lys33 was recognized as neutral states according to pK_a calculation (Tables S1). The partial charges of Thr1 and Lys33 were calculated using methods similar to those of the above inhibitor. The simulation system was solved using MOLARIS-XG and was then energy minimized to remove bad contacts under the ENZYMIX force field.[30]

EVB Simulations.

Before the EVB simulations, the simulation system was equilibrated thoroughly. Initially, the system was relaxed via a multistep heating procedure with a large constraint force on the reacting atoms and then gradually released the constraint under 300 K. The heating procedure increased the temperature in nine steps from 1 to 300 K with increments of 40 K, and the increment was 20 K from 280 to 300 K. Each temperature relaxed 20 ps, and the heating process lasted 180 ps. During heating, the reacting atoms in region I were constrained using force with 50 kcal/mol/Å^2. This constraint was then released in six steps from 50 to 0.3 in 10 kcal/mol/Å^2 decrements for a total of 120 ps. Later, the system was equilibrated in an additional 300 ps. Three starting conformations of EVB calculations were generated from the final equilibration. The system was immersed in a 22 Å sphere of water molecules, and a 2 Å spherical shell of Langevin dipoles was further surrounded. In the EVB calculations, each reaction simulated 11 frames from the reactant to product. Each frame was run for 10 ps. To obtain the calibration parameters of the gas phase shift and coupling constant, the reference reaction in water was conducted using the same parameters in the protein system. The partial charges of EVB atoms and all other EVB parameters are provided in the Supporting Information. The reported energies in the free energy profile were averaged from three independent EVB simulations.

PDLD/S-LRA/β Simulations.

The PDLD/S-LRA/β simulations were used to obtain the noncovalent binding energy of the inhibitor. The starting conformation of the system was generated by using the same way in the EVB simulations. The ionization states of all the titratable residues were determined through the POLARIS module in MOLARIS-XG.[31–33] This approach to determining the pK_a's of ionizable residues in proteins is described in detail in refs 31 and 32. In the PDLD/ S-LRA/β simulation, the linear response approximation (LRA) calculation was performed on 20 different protein configurations. The presented results were averaged from five independent simulations.

Kinetic Assays.

The human 20S proteasome (E-360, R&D Systems) diluted in reaction buffer (50 mM HEPES, 1 mM DTT, 1 mM EDTA, pH 7.6) at a final concentration of 0.0365 mg/mL was added to blank 96-well plates, and then a testing inhibitor with various concentrations and the final concentration of 20 μM fluorogenic substrate Suc-LLVY-AMC (S-280, Boston Biochem) were added immediately. The relative fluorescence units (RFU) were measured by a PerkinElmer EnVision multimode plate reader with an excitation wave-length of 345 nm and an emission wavelength of 445 nm every 3 min for 2 h.

RESULTS AND DISCUSSION

pK_a Calculation.

The initial ionization states of the amino acid residues in the catalytic center play a vital role in driving the inhibition mechanism. Thus, pK_a calculations were first performed to evaluate the ionization states of the groups. According to the calculated pK_a values (Tables S1), the NH_2 group of Thr1 along with the side chains (e.g., Lys33 and Asp17) are all deprotonated. These results imply that Lys33 could be a proton acceptor and participates in the proton transfer process. It supports the widely accepted scenario that Lys33 initiates the reaction by deprotonating the Thr1 hydroxyl group[20–23]

Calculating the Noncovalent Binding Free Energy (ΔG_{noncov}).

According to the ordering of the PT1 and the inhibitor noncovalent binding, we calculated the ΔG_{noncov} values of two noncovalent complexes. In one case, the noncovalent binding of the inhibitor occurs in the neutral form (i.e., before the PT1 from Thr1 to Lys33) as designated by the "NoncovPNP pathway" (noncov → PT1 → NA2 → PT3) in Figure 2. In another case, the noncovalent binding of the inhibitor happens in the ionized form (i.e., after the PT1 from Thr1 to Lys33) as designated by "PnoncovNP" (PT1 → noncov → NA2 → PT3) and "PnoncovPNP" (PT1 → noncov → PT2 → NA3 →PT4) pathways in Figure 2. In both cases, we obtained similar binding free energies (−4.8 kcal/mol for the first case and −4.1 kcal/mol for the second case). In a recent report, we estimated the ΔG_{noncov} of the inhibitor–protein bound complex (−4.3 kcal/mol) that is similar to the current result.[34] These results indicate that the ionization of Thr1 and Lys33 has little effect on the formation of the inhibitor–protein noncovalent complex. To clarify the structure–activity relationship, we analyzed the energy contributions of each residue toward the total binding free energy.

These plots (Figure S1) identify a significant contribution from three residues: Thr21, Gly47, and Ala49. All three residues form hydrogen bonds with the peptide backbone of the inhibitors (Figure 1), which constitutes the "hot spots" for the chymotrypsin-like site of the proteasome, and the hydrogen bonds play a vital role in the noncovalent binding.

Calculating the Reaction Free Energy of the First Proton Transfer Step (ΔG_{PT1}).

In the PT1, the hydroxyl group of Thr1 is deprotonated and Lys33 accepts the proton, forming an ammonium structure (NH_3^+) (Figure 3). The PT1 reaction between Thr1 and Lys33 was calculated in two situations, i.e., in apo and holo enzymes. The reference reactions in water were also performed in the presence or absence of the inhibitor. In the presence of the inhibitor, the $\Delta G_{PT1,obs}$ of 8.0 kcal/mol was taken from Figure 8 in ref 35. In the absence of the inhibitor, the $\Delta G_{PT1,obs}$ was calculated from the pK_a difference between Lys and Thr residues based on eq 1.[35,36] Here, the calculated values for the pK_a's of hydroxyl in Thr1 and the NH_2 group in Lys33 are 13.84 and 4.98, respectively (Tables S1). $\Delta G_{PT1,obs}$ is then determined as $\Delta G_{PT1,obs} = 1.36 \times (pK_{a\text{-}OH,Thr1} - pK_{a\text{-}NH2,Lys33}) = 1.36 \times (13.84–4.98) = 12.0$ kcal/mol. We used this as the reference reaction value in water to calibrate the reaction in a protein environment without the inhibitor. The two situations (e.g., apo and holo enzymes) generated a remarkable difference in the PT1 profiles having a reaction free energy of 9.1 kcal/mol for the Pnoncov pathway and 12.9 kcal/mol for the NoncovP pathway. From these results, we predict that the reaction happens in the absence of an inhibitor since it has a much lower energy penalty. We infer that the presence of the inhibitor probably has unfavorable steric and polar effects on the PT1 step. This result is in agreement with the conclusion of ref 26, which investigated the inhibition mechanism of a cysteine protease by an α-ketoamide inhibitor using the EVB approach.[26]

$$\Delta G_{PT} = 2.3RT(pK_{aAH} - pK_{aBH}) \quad (1)$$

where R is the universal gas constant, T is the absolute temperature, and AH and BH denote a proton donor (AH) and acceptor (BH), respectively.

We further compared the average distances of the reacting heavy atoms (OG1 and NZ) between Thr1 and Ly33 during the equilibration phase (see Table 1). The system without the inhibitor (labeled with "nolig" in Table 1) had a shorter distance (2.84 Å) and lower activation energies than the system with the inhibitor (3.37 Å). Figure 4 presents the structures of the reactants and products of both pathways. The distances between the carboxyl group of Asp17 and the amino group of Lys33 were also investigated. In the absence of the inhibitor, Asp17 forms a more stabilized electrostatic interaction with Lys33 considering the shorter distances between NZ and OD1/OD2. Reducing the ionization strength of Asp17 (say hi17 and ni17 in Table 1) results in longer distances between the atoms and higher activation energies. These results suggest that Asp17 has an important role in the reaction, and Asp17's polar effect probably makes Lys33 more easily accept the proton from Thr1. Therefore, we investigated the effect of different ionization states of Asp17 in the following reaction steps.

Calculating the Reaction Free Energy of the Second Proton Transfer Step (ΔG_{PT2}).

In PT2, the amino group of Thr1 accepts a proton from the ammonium group of Lys33. PT2 is involved in the PnoncovPNP pathway, which is similar to what was proposed to be the lowest energy pathway for substrate hydrolysis.[23] We estimated the $\Delta G^{\#}_{PT2,\,obs}$ in a water environment (1.6 kcal/mol) that was then used to calibrate the reaction in protein yielding a value of 1.3 kcal/mol (see Table S2).

Calculating the Activation and Reaction Free Energies of the Nucleophilic Attack ($\Delta G^{\#}_{NA}$ and ΔG_{NA}).

In the NA step, the activated anionic O^{γ} atom of Thr1 attacks the α-keto group of the inhibitor and yields an anionic tetrahedral complex. The NA reaction was also calculated under two circumstances according to whether there was a PT2 step between Lys33 and Thr1 (see PnoncovNP and PnoncovPNP pathways in Figure 2). In the PnoncovNP pathway, the NA2 step occurs right after the inhibitor binding, while in the PnoncovPNP pathway, the NA3 step occurs after the PT2 step. The reference numbers (e.g., activation energy ($\Delta G^{\#}_{NA,obs}$) of 16 kcal/mol and reaction free energy ($\Delta G_{na,\,obs}$) of 10 kcal/mol) for the NA step were taken from Figure 8 in ref 35. The calculated activation energies in the protein environment ($\Delta G^{\#}_{NA}$) are 14.29 and 19.66 kcal/mol for the NA2 and NA3 steps, respectively. These results reveal that NA2 has lower activation energy, implying PnoncovNP as a plausible reaction pathway. Figure 5 presents the structures of the reactants and products of the NA step for both pathways. From structural analysis, we observed that the distances between N (Thr1) and O4 (α-keto oxygen of the inhibitor) in the PnoncovPNP pathway (3.33 Å) are much smaller than the distances in the PnoncovNP pathway (4.26 Å) (see Table 2). It suggests that there is a stronger hydrogen bond interaction between the NH_3^+ group of Thr1 and the carbonyl group of the inhibitor (distance is 2.9 Å in Figure 5), which probably decreases the electrophilicity of the carbon atom in the α-keto group. The anionic O^{γ} atom of Thr1 attacks the carbon (in the case of NA3) with less electrophilicity that needs to overcome a higher barrier. Thus, the NA3 step that happens after the PT2 step has a higher reaction barrier, which makes the PnoncovPNP pathway less favorable.

We also investigated the effect of different ionization states of Asp17 on the kinetics and thermodynamics of the NA step. The average distance between the two reacting heavy atoms (i.e., OG1 (Thr1) and C24 (α-keto) in Table 2) is the shortest in the system with half-ionized ASP17 (hi17) for both the PnoncovNP (3.16 Å) and PnoncovPNP pathways (3.13 Å). However, the activation barrier is significantly lower in the case of NA2-hi17 (i.e., 14.29 kcal/mol) as compared to NA3-hi17 (i.e., 19.66 kcal/mol). Thus, we predict NA2-hi17 as the most favorable nucleophilic attack mechanism.

Calculation of the Reaction Free Energy of the Last Proton Transfer step (ΔG_{PT3}).

In the PT3 step, the anionic tetrahedral O4 atom of the inhibitor accepts a proton from the ammonium structure (NH_3^+) of Lys33. Here, we only considered the PT3 for the PnoncovNP pathway since it has a lower activation barrier as compared to the PnoncovPNP pathway in the NA step.

We used eq 1 to obtain $\Delta G_{\mathrm{PT3,\ obs}}$ for the reference reaction. The obtained $\Delta G_{\mathrm{PT3,\ obs}}$ in water was −10 kcal/mol considering the pK_a of amine (i.e., 4.80) and the pK_a of the tetrahedral intermediate (i.e., 12.13) (Tables S1). Using this as the reference value, we calculated the reaction free energy of the PT3 step in Table 3. The results indicate that the PT3 step contributes the maximum exergonicity as compared to any other steps. This implies that tuning the proton affinity of the tetrahedral complex (e.g., which can be achieved by placing suitable electron withdrawing or donating groups[37]) provides an effective way to design a reversible vs irreversible inhibitor.

The effect of different ionization states of Asp17 on PT3 is listed in Table 3. With un-ionized Asp17 (ni17), the average distance between the two reacting heavy atoms, NZ (Lys33) and O4 (α-keto), is shortest (2.92 Å) and the reaction free energy is the lowest. With reduced ionization strength of Asp17, the distance between Asp17 and Lys33 (NZ-OD1 and NZ-OD2) gets longer while the ΔG becomes lower. Thus, a strong electrostatic interaction between positively charged Lys33 and negatively charged Aspl7 may prohibit Lys33 to lend a proton to the tetrahedral complex. This implies that PT3 will occur at the un-ionized sate of Asp17.

To summarize, our calculations indicate that PnoncovNP is the most favorable covalent inhibition pathway (Figure 6) for the inhibitor Bsc2189, which has a calculated activation energy ($\Delta G^{\#}_{\mathrm{cov,cal}}$) and binding free energy ($\Delta G_{\mathrm{COV,\ cal}}$) of 19.3 and −11.6 kcal/mol, respectively.

$$E + \underset{k_{-1}}{\overset{k_1}{\rightleftharpoons}} E \times I \underset{k_{-2}}{\overset{k_2}{\rightleftharpoons}} E - I \tag{2}$$

$$P(t) = P_0 + V_s t - \frac{(V_s - V_0)\left(1 - \mathrm{e}^{-k_{\mathrm{obs}}t}\right)}{k_{\mathrm{obs}}} \tag{3}$$

$$K_{\mathrm{obs}} = \frac{k_2[I]}{(k_i + [I])} \tag{4}$$

$$k_2 = \frac{\mathrm{K_B}T}{h} e^{-E_a/RT} \tag{5}$$

$$\Delta G = RT \ln k_i$$

(6)

We also notice that PT1, NA2, and PT3 reaction steps will occur at the ionized, half-ionized, and un-ionized states of Asp 17. Thus, we conclude that the ionization state of Asp17 significantly changes along the reaction process to help guide it in the most energetically viable pathway.

Validation of the Calculated Activation and Reaction Binding Free Energy Through Kinetic Experiments.

To verify the calculated results, we performed kinetic experiments to obtain the experimental activation ($\Delta G^{\#}_{cov,exp}$) and binding free energy ($\Delta G_{cov,exp}$) of the inhibitor. The tested k_2 and k_i, ($k_i = k_{-1}/k_1$) values in the kinetic experiments (eq 3 and eq 4) could be used to determine the experimental activation energy (E_a or $\Delta G^{\#}_{cov,exp}$) based on the Transition State Theory (eq 5) and the binding free energy ($\Delta G_{cov,exp}$) according to eq 6, respectively.[15,38–40] Analysis of the progress curves of Figure 7 yielded a value of 0.01268 s^{-1} and a k_i value of 6.039 nM. Therefore, the experimental $\Delta G^{\#}_{cov,exp}$ and $\Delta G_{cov,exp}$ are 20.04 and −11.26 kcal/mol, respectively. The calculated $\Delta G^{\#}_{cov,exp}$ (19.3 kcal/mol) and $\Delta G_{cov,cal}$ (−11.6 kcal/mol) values are very close to the experimental values.

CONCLUSIONS

In this work, we investigated the inhibition mechanism of an *a*-ketoamide covalent inhibitor (Bsc2189) of the proteasome. We estimated the noncovalent contribution using the PDLD/S-LRA/β method and the covalent contribution using the EVB method. Our calculations examined multiple reaction pathways for the covalent adduct formation. The PnoncovNP pathway was recognized as the most plausible path. The calculated activation and reaction free energies were verified by kinetic experiments. The results indicate that the nucleophilic attack step is the rate-determining step, which occurs after the PT1 and noncovalent binding. We also notice that the PT3 step contributes to the maximum exergonicity. This suggests that the electrophilicity of the warhead of the inhibitor and the proton affinity of the tetrahedral complex in the PT3 step play important roles and thus should be exploited during SAR to optimize the inhibitor for better activity.

Analysis of the ionization effect of Asp17 on the calculated activation energies and the distances of reacting atoms in each reaction step revealed that different ionization states of Asp17 could cause remarkable differences in results. Interestingly, it appears that the ionization state of Asp17 probably changes along the reaction. In the PT1 step, Asp17 is in the ionized state, which helps to stabilize the positively charged product (e.g., $NH3^+$ group in Lys33). In contrast, in the PT3 step, Asp17 is in un-ionized state since Lys33 is reverting to its neutral form. This result suggests that the ionization states of Aspl7 and Lys33 are affected by each other due to the strong electrostatic interactions. Thus, we conclude that Asp17 plays a vital catalytic role in the active site of the proteasome and Thrl–Aspl7–Lys33 constitutes a catalytic triad. The importance of Asp17 revealed here is in agreement with a recently reported work in which the authors performed an electrostatic potential analysis and showed that the Asp17–Lys33 dyad plays a critical role in the irreversible inhibition

of proteasome by salinosporamide A (SalA).[24] Our results demonstrate an electrostatic reorganization in the catalytic center of the 20S proteasome along the reaction, which could be considered when studying the inhibition mechanism of covalent proteasomal inhibitors.

Supplementary Material

Refer to Web version on PubMed Central for supplementary material.

ACKNOWLEDGMENTS

This work was supported in part by the Ganghong Young Scholar Development Fund and fund from Shenzhen-Hong Kong Cooperation Zone for Technology and Innovation (HZQB-KCZYB-2020056), and the National Institute of Health R35 GM12247. We also thank the University of Southern California Zumberge award and the University of Southern California High Performance Computing and Communication Center for computational resources.

REFERENCES

(1). Nandi D; Tahiliani P; Kumar A; Chandu D The Ubiquitin-Proteasome System. j. Biosci 2006, 31 (1), 137–155. [PubMed: 16595883]

(2). Murata S; Yashiroda H; Tanaka K Molecular Mechanisms of Proteasome Assembly. Nat. Rev. Mol. Cell Biol 2009, 10 (2), 104–115. [PubMed: 19165213]

(3). Collins GA; Goldberg AL The Logic of the 26S Proteasome. Cell 2017, 169 (5), 792–806. [PubMed: 28525752]

(4). Lee AH; Iwakoshi NN; Anderson KC; Glimcher LH Proteasome Inhibitors Disrupt the Unfolded Protein Response in Myeloma Cells. Proc. Natl. Acad. Sci. U.S.A 2003, 100 (17), 9946–9951. [PubMed: 12902539]

(5). Gandolfi S; Laubach JP; Hideshima T; Chauhan D; Anderson KC; Richardson PG The Proteasome and Proteasome Inhibitors in Multiple Myeloma. Cancer Metastasis Rev 2017, 36 (4), 561–584. [PubMed: 29196868]

(6). Fricker LD Proteasome Inhibitor Drugs. Annu. Rev. Pharmacol. Toxicol 2020, 60, 457–476. [PubMed: 31479618]

(7). Wang J; Liang B; Chen Y; Fuk-Woo Chan J; Yuan S; Ye H; Nie L; Zhou J; Wu Y; Wu M; Huang LS; An J; Warshel A; Yuen K-Y; Ciechanover A; Huang Z; Xu Y A New Class of a-Ketoamide Derivatives with Potent Anticancer and Anti-SARS-CoV-2 Activities. Eur. J. Med. Chem 2021, 215, No. 113267. [PubMed: 33639344]

(8). Stein ML; Cui H; Beck P; Dubiella C; Voss C; Krüger A; Schmidt B; Groll M Si-Systematic Comparison of Peptidic Proteasome Inhibitors Highlights the α-Ketoamide electrophile as an Auspicious Reversible Lead Motif. Angew. Chem. - Int. Ed 2014, 53 (6), 1679–1683.

(9). Stubba D; Bensinger D; Steinbacher J; Proskurjakov L; Salcedo Gomez Á; Schmidt U; Roth S; Schmitz K; Schmidt B Cell-Based Optimization of Covalent Reversible Ketoamide Inhibitors Bridging the Unprimed to the Primed Site of the Proteasome B5 Subunit. ChemMedChem 2019, 14 (23), 2005–2022. [PubMed: 31675179]

(10). Voss C; Scholz C; Knorr S; Beck P; Stein ML; Zall A; Kuckelkorn U; Kloetzel PM; Groll M; Hamacher K; Schmidt B α-Keto Phenylamides as P1'-Extended Proteasome Inhibitors. ChemMedChem 2014, 9 (ll), 2557–2564. [PubMed: 25087721]

(11). Rusere LN; Lockbaum GJ; Lee SK; Henes M; Kosovrasti K; Spielvogel E; NaUvaika EA; Swanstrom R; Yilmaz NK; Schiffer CA; Ali A HIV-1 Protease Inhibitors Incorporating Stereochemically Defined P2' Ligands to Optimize Hydrogen Bonding in the Substrate Envelope. J. Med. Chem 2019, 62 (17), 8062–8079. [PubMed: 31386368]

(12). Ganesan R; Jelakovic S; Campbell AJ; Li ZZ; Asgian JL; Powers JC; Grütter MG Exploring the S4 and SI Prime Subsite Specificities in Caspase-3 with Aza-Peptide Epoxide Inhibitors. Biochemistry 2006, 45 (30), 9059–9067. [PubMed: 16866351]

(13). Ingallinella P; Fattori D; Altamura S; Steinkühler C; Koch U; Cicero D; Bazzo R; Cortese K; Bianchi E; Pessi A Prime Site Binding Inhibitors of a Serine Protease: NS3/4A of Hepatitis C Virus. Biochemistry 2002, 41 (17), 5483–5492. [PubMed: 11969409]

(14). Stein ML; Cui H; Beck P; Dubiella C; Voss C; Krüger A; Schmidt B; Groll M Systematic Comparison of Peptidic Proteasome Inhibitors Highlights the α-Ketoamide electrophile as an Auspicious Reversible Lead Motif. Angew. Chem. - Int. Ed 2014, 53 (6), 1679–1683.

(15). De Cesco S; Kurian J; Dufresne C; Mittermaier AK; Moitessier N, Covalent Inhibitors Design and Discovery. Eur. J. Med. Chem 2017, 138, 96–114. [PubMed: 28651155]

(16). Wei D; Lei B; Tang M; Zhan CG Fundamental Reaction Pathway and Free Energy Profile for Inhibition of Proteasome by Epoxomicin. J. Am. Chem. Soc 2012, 134 (25), 10436–10450. [PubMed: 22697787]

(17). Wei D; Fang L; Tang M; Zhan CG Fundamental Reaction Pathway for Peptide Metabolism by Proteasome: Insights from First-Principles Quantum Mechanical/Molecular Mechanical Free Energy Calculations. J. Phys. Chem. B 2013, 117 (4300), 13418–13434. [PubMed: 24111489]

(18). Wei D; Tang M; Zhan CG Fundamental Reaction Pathway and Free Energy Profile of Proteasome Inhibition by Syringolin A (SylA). Org. Biomol. Chem 2015, 13 (24), 6857–6865. [PubMed: 26018983]

(19). Huber EM; Heinemeyer W; Li X; Arendt CS; Hochstrasser M; Groll M A Unified Mechanism for Proteolysis and Autocatalytic Activation in the 20S Proteasome. Nat. Commun 2016, 7 (1), 1–10.

(20). Serrano-Aparicio N. j Moliner V; Świderek K On the Origin of the Different Reversible Characters of Salinosporamide A and Homosalinosporamide A in the Covalent Inhibition of TheHuman20S Proteasome. ACS Catal 2021, 11 (18), 11806–11819.

(21). Mihalovits LM; Ferenczy GG; Keserű GM Mechanistic and Thermodynamic Characterization of Oxathiazolones as Potent and Selective Covalent Immunoproteasome Inhibitors. Comput. Struct. Biotechnol. J 2021, 19, 4486–4496. [PubMed: 34471494]

(22). Serrano-Aparicio N; Świderek K; Moliner V Theoretical Study of the Inhibition Mechanism of Human 20S Proteasome by Dihydroeponemycin. Eur. J. Med. Chem 2019, 164, 399–407. [PubMed: 30611981]

(23). Saha A; Oanca G; Mondal D; Warshel A Exploring the Proteolysis Mechanism of the Proteasomes. J. Phys. Chem. B 2020, 124, 5626–5635. [PubMed: 32498514]

(24). Serrano-Aparicio N; Moliner V; Świderek K Nature of Irreversible Inhibition of Human 20S Proteasome by Salinosporamide The Critical Role of Lys-Asp Dyad Revealed from Electrostatic Effects Analysis. ACS Catal 2021, 11 (6), 3575–3589.

(25). Warshel A; Weiss RM An Empirical Valence Bond Approach for Comparing Reactions in Solutions and in Enzymes. J. Am. Chem. Soc 1980, 102 (20), 6218–6226.

(26). Mondal D; Warshel A Exploring the Mechanism of Covalent Inhibition: Simulating the Binding Free Energy of α-Ketoamide Inhibitors of the Main Protease of SARS-CoV-2. Biochemistry 2020, 59 (48), 4601–4608. [PubMed: 33205654]

(27). Akintola O; Farren-Dai M; Ren W; Bhosale S; Britton R; Świderek K; Moliner V; Bennet AJ Glycoside Hydrolase Catalysis: Do Substrates and Mechanism-Based Covalent Inhibitors React via Matching Transition States? ACS Catal 2022, 12 (23), 14667–14678.

(28). Frisch M; Trucks GW; Schlegel HB; Scuseria GE; Robb MA; Cheeseman JR; Scalmani G; Barone V; Mennucci B; Petersson Ga. Gaussian 09, Revision d. 01; Gaussian. Inc.: Wallingford CT, 2009, 201.

(29). Bayly CI; Cieplak P; Cornell W; Kollman PA A Well-Behaved Electrostatic Potential Based Method Using Charge Restraints for Deriving Atomic Charges: The RESP Model. J. Phys. Chem 1993, 97 (40), 10269–10280. ‘

(30). Lee FS; Chu ZT; Warshel A Microscopic and Semimicroscopic Calculations of Electrostatic Energies in Proteins by the POLARIS and ENZYMIX Programs. J. Comput. Chem 1993, 14 (2), 161–185.

(31). Warshel A Calculations of Enzymic Reactions: Calculations of PKa, Proton Transfer Reactions, and General Acid Catalysis Reactions in Enzymes. Biochemistry 1981, 20 (ll), 3167–3177. [PubMed: 7248277]

(32). Sham YY; Chu ZT; Warshel A Consistent Calculations of p K a's of Ionizable Residues in Proteins: Semi-Microscopic and Microscopic Approaches. J. Phys. Chem. B 1997, 101 (22), 4458–4472. '

(33). Warshel A; Chu ZT; Villa J; Strajbl M; Schutz CN; Shurki A; Vicatos S; Plotnikov NV; Schopf P Molaris-XG, v 9.15 University of Southern California, Los Angeles Warshel Group 2012.

(34). Zhou J; Saha A; Huang Z; Warshel A Fast and Effective Prediction of the Absolute Binding Free Energies of Covalent Inhibitors of SARS-CoV-2 Main Protease and 20S Proteasome. J. Am. Chem. Soc 2022, 144 (17), 7568–7572. [PubMed: 35436404]

(35). Štrajbl M; Florián J; Warshel A Ab Initio Evaluation of the Potential Surface for General Base-Catalyzed Methanolysis of Formamide: A Reference Solution Reaction for Studies of Serine Proteases. J. Am. Chem. Soc 2000, 122 (22), 5354–5366.

(36). Ŝtrajbl M; Florián J; Warshel A Ab Initio Evaluation of the Free Energy Surfaces for the General Base/Acid Catalyzed Thiolysis of Formamide and the Hydrolysis of Methyl Thiolformate: A Reference Solution Reaction for Studies of Cysteine Proteases. J. Phys. Chem. B 2001, 105 (19), 4471–4484.

(37). Krenske EH; Petter RC; Houk KN Kinetics and Thermodynamics of Reversible Thiol Additions to Mono- and Diactivated Michael Acceptors: Implications for the Design of Drugs That Bind Covalently to Cysteines. J. Org. Chem 2016, 81 (23), 11726–11733. [PubMed: 27934455]

(38). Lin G; Li D; Chidawanyika T; Nathan C; Li H Fellutamide B Is a Potent Inhibitor of the Mycobacterium Tuberculosis Proteasome. Arch. Biochem. Biophys 2010, 501 (2), 214–220. [PubMed: 20558127]

(39). Hasinoff BB Progress Curve Analysis of the Kinetics of Slow-Binding Anticancer Drug Inhibitors of the 20S Proteasome. Arch. Biochem. Biophys 2018, 639, 52–58. [PubMed: 29305052]

(40). Ma C; Sacco MD; Hurst B; Townsend JA; Hu Y; Szeto T; Zhang X; Tarbet B; Marty MT; Chen Y; Wang J Boceprevir, GC-376, and Calpain Inhibitors II, XII Inhibit SARS-CoV-2 Viral Replication by Targeting the Viral Main Protease. Cell Res 2020, 30 (8), 678–692. [PubMed: 32541865]

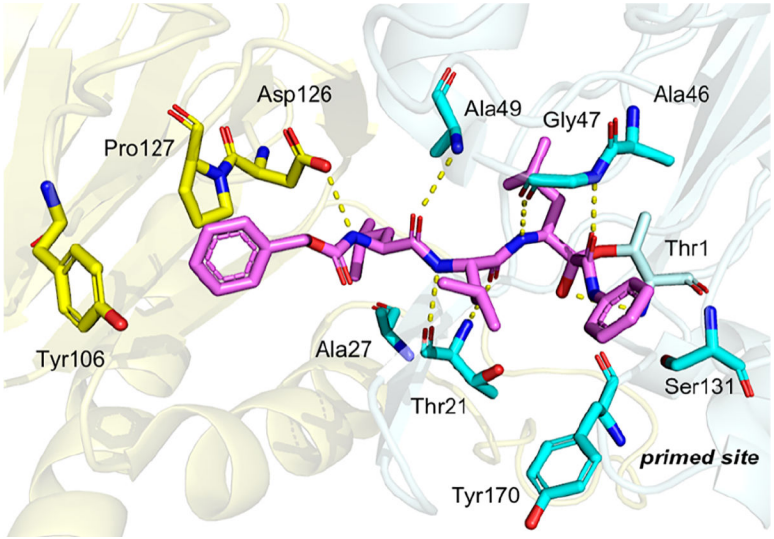

Figure 1.

Binding mode of the α-ketoamide BSc2189 in the substrate-binding cleft located between β5 and β6 subunits of the proteasome (PDB code: 4N08).

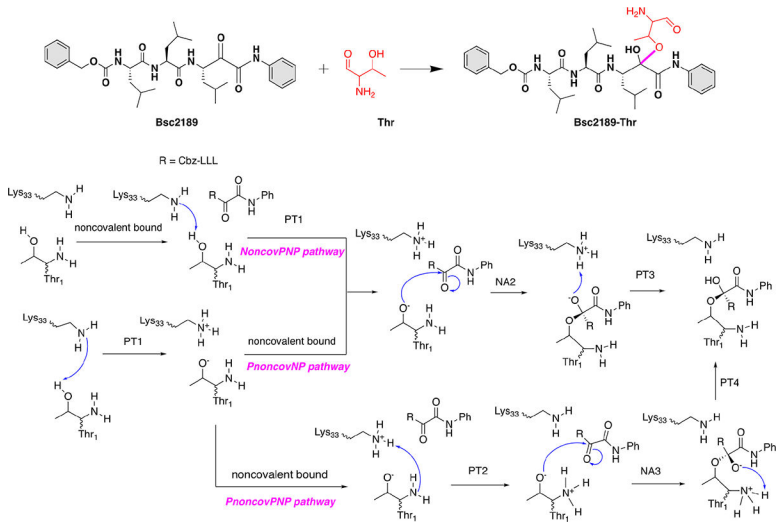

Figure 2.

Three proposed reaction mechanisms for Bsc2189 covalent inhibition. PT1 stands for first proton transfer, PT2 stands for second proton transfer, PT3 stands for third proton transfer, NA2 stands for the nucleophilic attack step after PT1, and NA3 stands for the nucleophilic attack step after PT2.

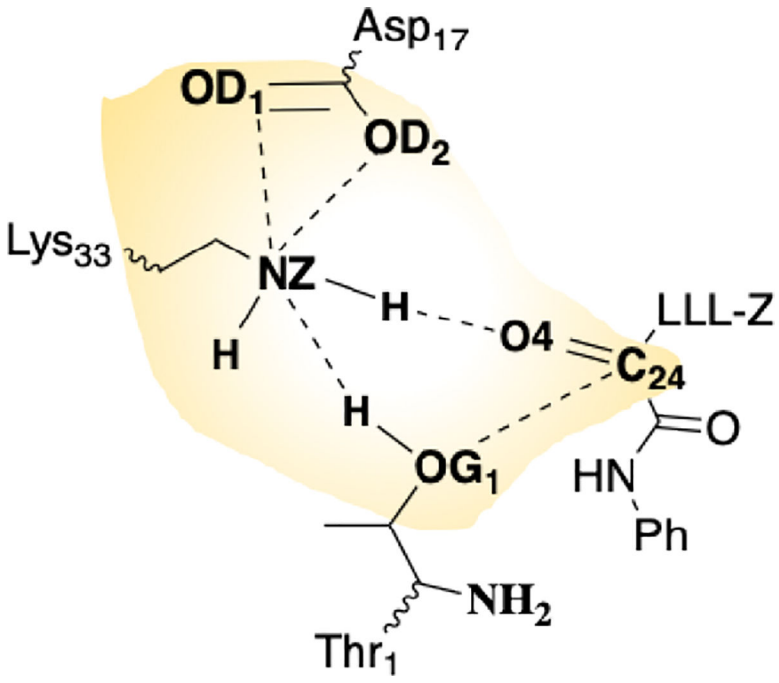

Figure 3.
Structure of the active site of the β5 subunit of the human 20S proteasome

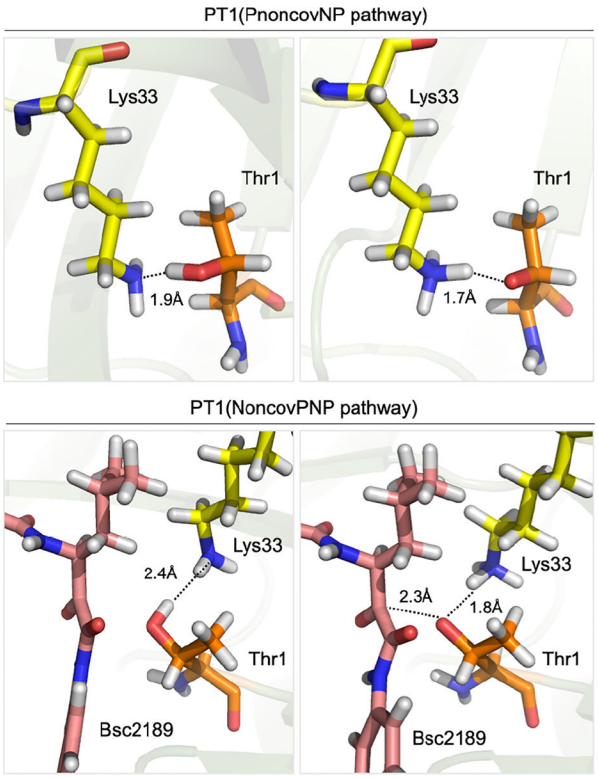

Figure 4.
Structures before (left, reactant) and after (right, product) the PT1 reaction for the PnoncovNP pathway, and the NoncovPNP pathway.

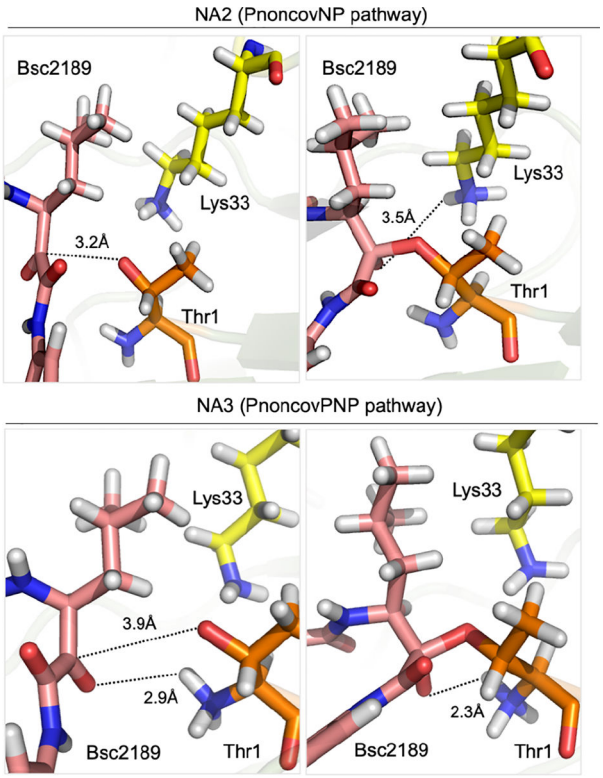

Figure 5.
Structures before (left) and after (right) the NA reaction for the PnoncovNP pathway and the PnoncovPNP pathway.

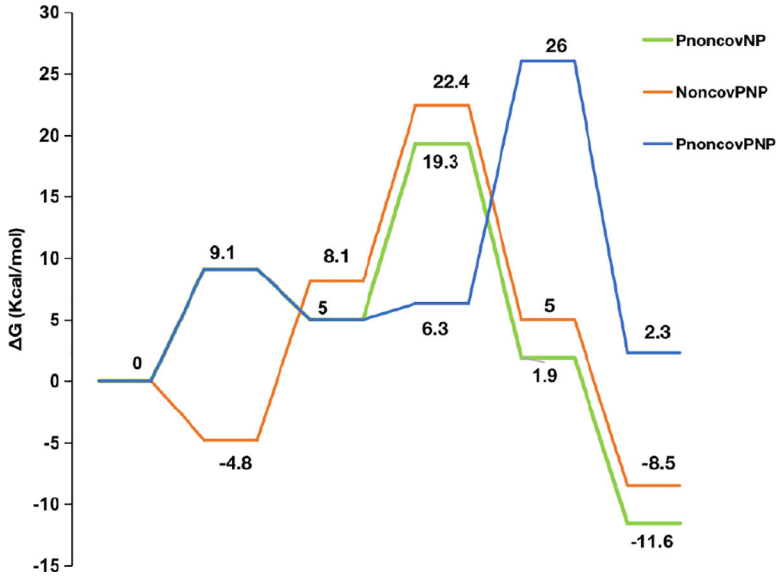

Figure 6.

Calculated free energy surface (FES) of formation of the covalent proteasome-Bsc2189 complex.

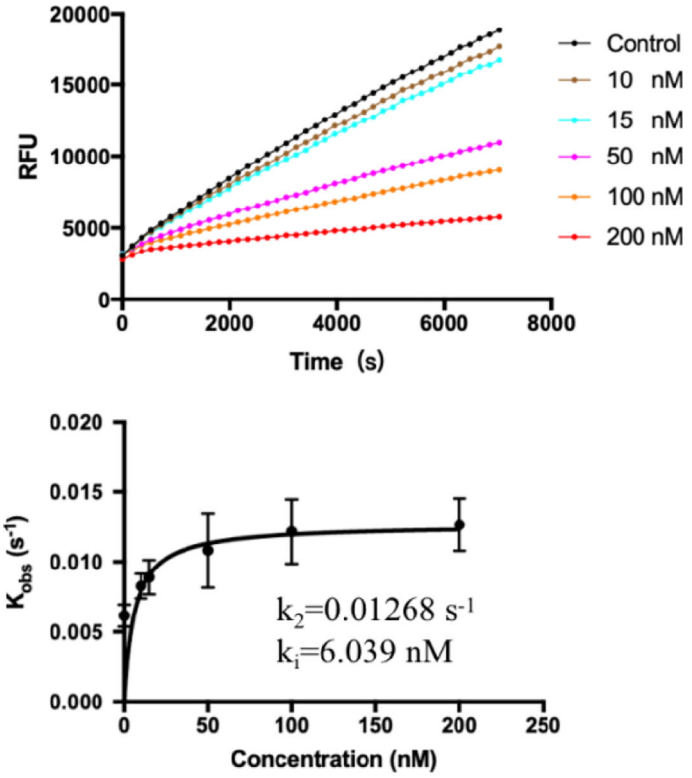

Figure 7.

Results of kinetic experiments. The upper column shows the reaction progress curve of hydrolysis of Suc-LLVY-AMC by the 20S proteasome in the presence of Bsc2189 at 0–200 nM. The curves were fit to eq 3 to determine the apparent k_{obs}. The below column shows the plot of k_{obs} values to [Bsc2189]. Fitting to eq 4 yields k_i and k_2. The activation energy E_a can be obtained according to the Transition State Theory in eq 5.

Table 1.

Average Distances among Key Atoms and Calculated Binding Free Energies of the PT1 Reaction with Different Ionization States for Asp 17[a]

	distance (Å)			ΔG_{cal} (kcal/mol)	
system	**NZ-OG1**	**NZ-OD1**	**NZ-OD2**	$\Delta G^{\#}$	ΔG
PT1-i17-lig	3.37	4.85	3.36	12.86	12.66
PT1-hi17-lig	3.19	4.54	5.72	19.22	18.81
PT1-ni17-lig	3.15	4.28	5.57	25.00	25.00
PT1-i17-nolig	2.84	3.06	3.08	9.09	9.09
PT1-hi17-nolig	2.94	4.39	3.69	12.52	12.52
PT1-ni17-nolig	2.95	3.89	5.08	11.11	11.11

[a]i17 represents ionres 17, and the net charge of the residue is −1; hi17 represents ionres_half 17, and the net charge of the residue is −0.5; ni17 represents without ionres 17, and the net charge of the residue is 0. -lig means there is a ligand in the system; -nolig means there is not a ligand in the system.

Table 2.

Average Distances among Key Atoms and Calculated Binding Free Energies of the NA Reaction with Different Ionization States for Asp17

	distance (Å)						ΔG_{cal} (kcal/mol)	
system	**NZ-OG1**	**NZ-OD1**	**NZ-OD2**	**OG1-C24**	**NZ-)O4**	**N–O4**	**$\Delta G^{\#}$**	**ΔG**
NA2-i17	3.02	2.99	3.01	3.33	6.8	5.26	14.29	5.33
NA2-hi17	3.11	3.23	3.34	3.16	3.75	4.26	14.29	−3.13
NA2-ni17	2.98	4.28	5.18	3.23	4.14	4.20	14.10	0.55
system	N-OG1	N-OD1	N-OD2	OG1-C24	NZ-O4	N-O4	$\Delta G^{\#}$	ΔG
NA3-i17	3.03	3.11	2.96	3.46	5.15	5.11	17.01	−2.69
NA3-hi17	2.94	5.37	4.36	3.13	5.63	3.33	19.66	−4.04
NA3-ni17	2.88	4.68	5.35	3.5	4.61	3.49	18.75	−2.85

Table 3.

Average Distances among Key Atoms and Calculated Binding Free Energies of the PT3 Reaction with Different Ionization States for Asp17

	distance (Å)				ΔG_{cal} (kcal/mol)	
system	**NZ-O4**	**NZ-N**	**NZ-OD1**	**NZ-OD2**	$\Delta G^{\#}$	ΔG
PT3-i17	4.35	4.18	2.93	3.06	0.50	−9.93
PT3-hi17	3.03	4.74	3.17	3.19	1.36	−12.39
PT3-ni17	2.92	4.29	3.88	4.73		−13.48